nature genetics

XPF nuclease-dependent telomere loss and increased DNA damage in mice overexpressing TRF2 result in premature aging and cancer

Purificación Muñoz[1,3], Raquel Blanco[1,3], Juana M Flores[2] & María A Blasco[1]

TRF2 is a telomere-binding protein that has a role in telomere protection. We generated mice that overexpress TRF2 in the skin. These mice had a severe phenotype in the skin in response to light, consisting of premature skin deterioration, hyperpigmentation and increased skin cancer, which resembles the human syndrome xeroderma pigmentosum. Keratinocytes from these mice were hypersensitive to ultraviolet irradiation and DNA crosslinking agents. The skin cells of these mice had marked telomere shortening, loss of the telomeric G-strand overhang and increased chromosomal instability. Telomere loss in these mice was mediated by XPF, a structure-specific nuclease involved in ultraviolet-induced damage repair and mutated in individuals with xeroderma pigmentosum. These findings suggest that TRF2 provides a crucial link between telomere function and ultraviolet-induced damage repair, whose alteration underlies genomic instability, cancer and aging. Finally, we show that a number of human skin tumors have increased expression of TRF2, further highlighting a role for TRF2 in skin cancer.

Telomeres are heterochromatic regions at the end of chromosomes that consist of tandem TTAGGG repeats and associated proteins[1,2]. Telomeric chromatin can be remodeled into a structure known as the T loop, which protects the single-stranded 3′ chromosome end (G-strand overhang) from degradation and repair activities[1,3]. The proper function of telomeres is essential for chromosome stability and cell viability[1,4]. Telomere shortening or loss of function of telomere-binding proteins results in loss of telomere protection, end-to-end chromosome fusions and cell-cycle arrest or apoptosis[4,5].

The telomere-binding protein TRF2 is a crucial player in telomere protection and is involved in facilitating the formation of T loops[1,3,6]. TRF2 localizes to double-strand breaks after DNA damage[7] and interacts with proteins involved in various DNA repair pathways, including nonhomologous end-joining[8], base excision repair (PARP2)[9] and nucleotide excision repair (NER; ERCC1-XPF complex)[10]. The current view is that TRF2 represses these different DNA repair activities at telomeres, thereby providing telomere protection[3,6,11]. TRF2 expression is increased in various human tumors, suggesting that TRF2 may have a role in tumorigenesis[12,13].

To study the effect of TRF2 in the context of the organism, and in particular on cancer and aging, we generated *K5-Terf2* mice that express variable levels of TRF2 under control of the 5′ regulatory region of the bovine keratin K5 promoter[14], which targets TRF2 to basal cells and stem cells of the epidermis[15,16].

RESULTS

Premature aging and increased cancer in *K5-Terf2* mice

We obtained several founder transgenic mice (PM, PN and PO) with different levels of TRF2 expression in the skin. PM *K5-Terf2* mice had the highest *Terf2* mRNA expression (~59 times greater than wild-type), followed by PO (~23 times greater) and PN (~12 times greater) *K5-Terf2* mice (**Fig. 1a**). PO and PN *K5-Terf2* mice were born with normal mendelian distribution, but PM *K5-Terf2* males were born at a lower frequency than expected, suggesting that embryonic lethality was associated with high levels of TRF2 expression (**Supplementary Fig. 1** online). Primary keratinocytes from PM and PO *K5-Terf2* mice were less viable than those from wild-type controls (**Supplementary Fig. 1** and **Supplementary Methods** online). As expected, TRF2 protein levels were elevated in PM and PO *K5-Terf2* keratinocytes compared with wild-type cells (**Fig. 1b**). Combined TRF2 immunofluorescence and telomeric quantitative fluorescence *in situ* hybridization (Q-FISH) analysis showed that the overexpressed TRF2 protein localized to telomeres (**Fig. 1c**).

Macroscopic observation of transgenic mice showed hyperpigmentation of skin areas that are normally exposed to light, such as tail, paws and ears (**Fig. 2a**). The severity of this phenotype was proportional to TRF2 expression levels, being most acute in PM *K5-Terf2* mice (**Fig. 2a**). PM *K5-Terf2* mice eventually developed alopecia of the dorsal skin (**Fig. 2b**), accompanied by skin dryness (>78% of the cases) and hyperpigmentation (>30% of the cases), suggesting that

[1]Telomeres and Telomerase Group, Molecular Oncology Program, Spanish National Cancer Centre, Madrid, Spain. [2]Animal Surgery and Medicine Department, Facultad de Veterinaria, Universidad Complutense de Madrid, Madrid, Spain. [3]These authors contributed equally to this work. Correspondence should be addressed to M.A.B. (mblasco@cnio.es).

Received 24 March; accepted 26 July; published online 4 September 2005; doi:10.1038/ng1633

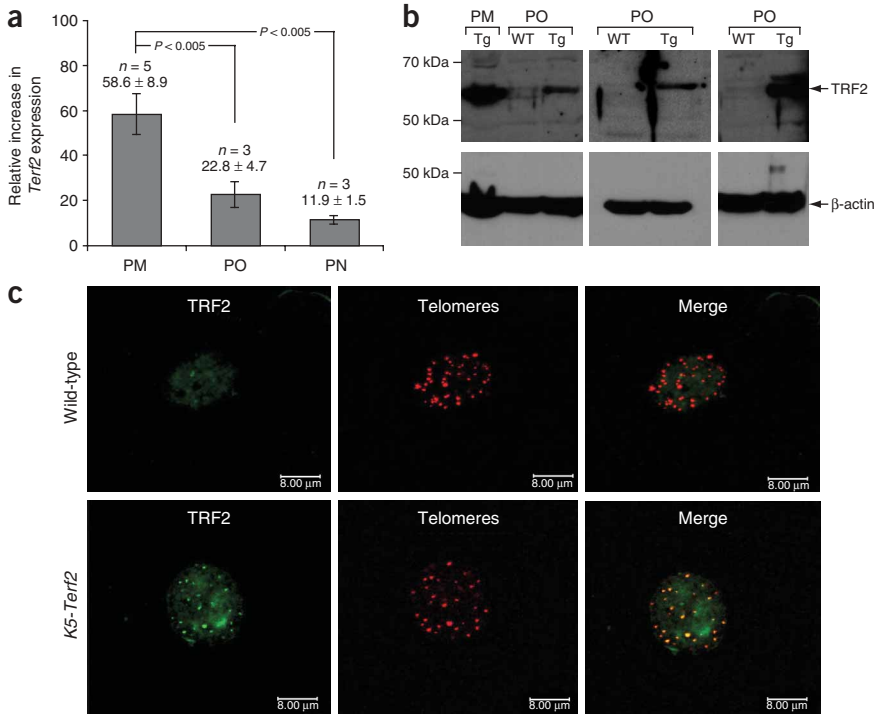

Figure 1 Increased TRF2 expression in *K5-Terf2* mice. (**a**) Quantification of *Terf2* mRNA in the skin (tail and back) of PM, PN and PO *K5-Terf2* mice compared with wild-type controls. Values are expressed as mean ± s.e. increase in *Terf2* levels in transgenic mice relative to nontransgenic mice. The PM transgenic line (males only) expressed significantly higher levels of *Terf2* mRNA than did the PO and PN lines (males and females; $P < 0.005$). The number of mice (n) and the mean ± s.e. increase in *Terf2* levels are indicated above each bar. (**b**) Quantification of TRF2 protein levels by western-blot analysis in wild-type (WT) and PM or PO *K5-Terf2* primary keratinocytes (Tg). (**c**) Overexpressed TRF2 goes to the nucleus and colocalizes with telomeres. TRF2 specific signal is shown in green; telomeric sequences as detected by Q-FISH are shown in red; colocalization is shown in yellow.

exposure to light triggered the appearance of the latter phenotypes. The severity of these phenotypes increased with age (**Fig. 2b**), indicating that increased TRF2 expression resulted in premature deterioration of the skin. Histopathological analysis of *K5-Terf2* mice showed that the tail skin had areas of epidermal atrophy, as well as atrophy of the hair follicles and the sebaceous glands (**Supplementary Fig. 2** online), in accordance with the hair loss and skin dryness phenotypes. The basal cell layer showed accumulation of melanin deposits (**Supplementary Fig. 2** online), in agreement with the skin hyperpigmentation phenotype. Light-exposed areas of the skin such as the tail and the ear also showed hyperplastic and dysplastic lesions (**Supplementary Fig. 2** online). These skin lesions were not found in age-matched wild-type controls (**Supplementary Fig. 2** online).

Older *K5-Terf2* mice developed spontaneous tumors in areas of the skin exposed to light, such as the tail (**Fig. 2c**). The incidence of these tumors increased with age (**Fig. 2d**). At >1 year of age, 23% and 50% of PO and PM *K5-Terf2* mice, respectively, had developed skin tumors in the tail, and some mice had multiple tumors (**Fig. 2c**). Histopathological analysis indicated that these tumors were keratoacanthomas and squamous cell carcinomas (SCCs; **Fig. 2c**). These findings suggest that increased TRF2 expression directly affects spontaneous skin carcinogenesis, in line with recent reports that TRF2 is upregulated in a number of human tumors[12,13].

Increased TRF2 expression in human skin cancer

To determine whether human skin tumors had elevated levels of TRF2 expression, we carried out real-time PCR analysis of human *TERF2* in a series of human primary tumors including 15 basal cell carcinomas (BCCs) and 3 SCCs and measured the relative change in *TERF2* mRNA in tumoral tissue compared with normal tissue (**Fig. 3a**). Five of 15 BCCs and 1 of 3 SCCs showed a reproducible increase (by a factor of 10–50) in *TERF2* levels relative to nontumoral tissue (**Fig. 3a**). Only one tumor (SCC 516; **Fig. 3a**) showed a substantial decrease in *TERF2* mRNA levels, suggesting that increased expression rather than loss of TRF2 is frequently associated with human skin carcinogenesis. For some tumors with increased (by a factor of ~10) *TERF2* mRNA expression (BCC 480.2 and SCC 509; **Fig. 3a**), confocal immunofluorescence analysis of paraffin-embedded tumor tissue with

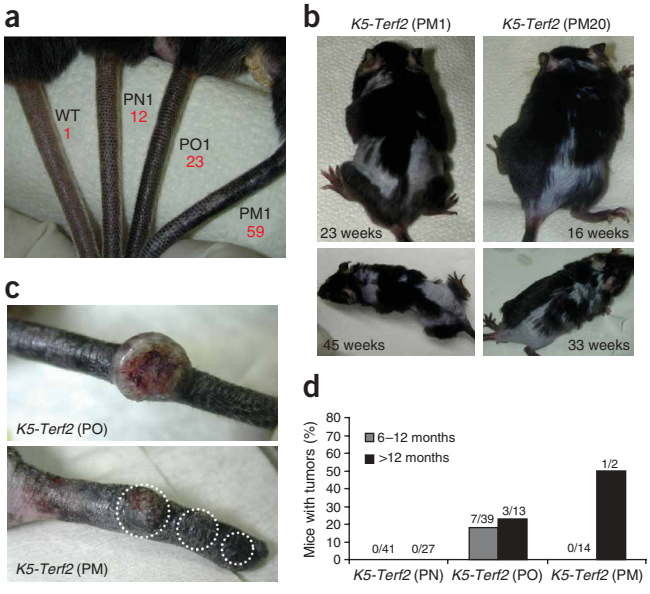

Figure 2 Skin phenotypes in *K5-Terf2* mice. (**a**) Representative images of tail hyperpigmentation in PM, PN and PO *K5-Terf2* mice. The relative expression of *Terf2* mRNA in transgenic mice compared with wild-type (WT) mice is indicated in red. Note that skin hyperpigmentation is more intense as TRF2 levels are higher. (**b**) Representative examples of progressive hair loss in two PM *K5-Terf2* mice. Phenotypes are aggravated with increasing age in both mice. (**c**) Spontaneous skin tumors in the tails of PO and PM *K5-Terf2* mice. A keratoacanthoma is shown in the PO mouse, and various SCCs are shown in the PM mouse. (**d**) Incidence of skin tumors with age in PO and PM transgenic mice.

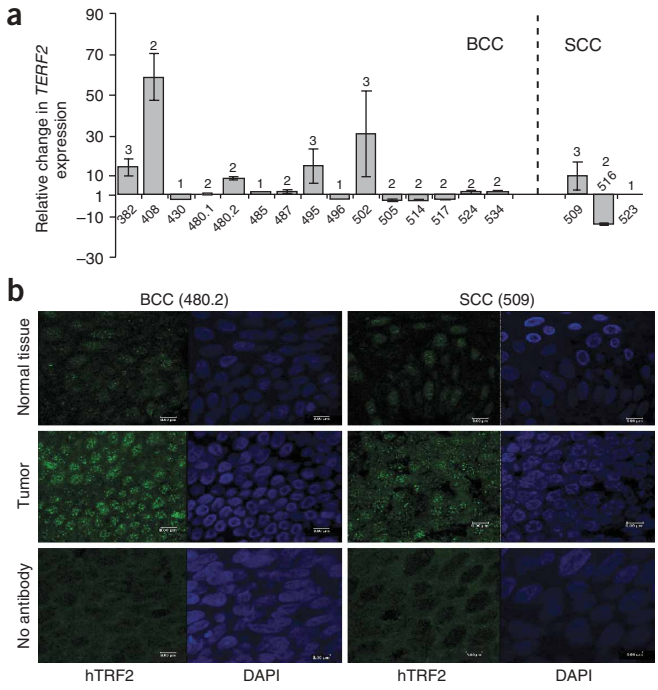

Figure 3 Increased *TERF2* expression in human skin tumors. (**a**) Relative change in expression of *TERF2* mRNA in the indicated human BCCs and SCCs compared with normal skin. Values shown are mean ± s.e. The number of independent RT-PCR reactions is shown above each bar. (**b**) Representative examples of confocal immunofluorescence with antibodies to human TRF2 (hTRF2) on paraffin sections from the indicated tumors. TRF2 staining is greater in tumors than in normal tissue.

antibodies to TRF2 showed that they had increased TRF2 fluorescence compared with the corresponding nontumoral tissue (**Fig. 3b**), confirming an increase in TRF2 expression in these tumors.

Ultraviolet-induced damage and carcinogenesis in *K5-Terf2* mice

The phenotypes of *K5-Terf2* mice are reminiscent of the skin phenotypes of the human syndrome xeroderma pigmentosum, which include skin hyperpigmentation, skin dryness, skin atrophies and increased skin cancer on exposure to sunlight[17,18]. Eight gene products are defective in individuals with xeroderma pigmentosum (XPA–XPG and XPV)[17,18], all components of the NER pathway[19,20] that removes ultraviolet (UV)-induced DNA lesions. TRF2 interacts with the NER ERCC1-XPF complex[10], a structure-specific nuclease that cuts 5′ of the DNA adducts during NER[19] and also has a role in eliminating interstrand DNA crosslinks[21]. ERCC1-XPF colocalizes with TRF2 at telomeres and is involved in G-strand processing[10]. Mice deficient for NER proteins are more susceptible to UV irradiation–induced damage and cancer[22–26].

To determine whether the skin phenotypes of *K5-Terf2* mice were due, at least in part, to increased damage in response to UV irradiation[17,18,20], we measured accumulation of UV-induced pyrimidine (6-4) photoproducts (6-4 PPs) and of cyclobutyl pyrimidine dimers (CPDs)[17,18,20] in UV-irradiated wild-type and *K5-Terf2* littermates. We observed an increase in CPDs and 6-4 PPs in PO and PM *K5-Terf2* mice compared with similarly irradiated wild-type mice (**Fig. 4a,b**). To confirm that *K5-Terf2* mice suffered more UV-induced DNA damage, we studied the susceptibility of *K5-Terf2* primary keratinocytes to UVB irradiation. As a control, we used *Xpa*-deficient mouse embryonic fibroblasts, which were hypersensitive to UV irradiation, as indicated by their decreased viability relative to wild-type controls (**Fig. 4c**)[25]. PO and PM *K5-Terf2* keratinocytes also showed decreased viability relative to wild-type controls after UVB irradiation (**Fig. 4c**), indicative of their hypersensitivity to UVB light.

Next, we studied the sensitivity of *K5-Terf2* keratinocytes to treatment with mitomycin C (MMC), which specifically decreases viability of ERCC1- or XPF-deficient cells[21,23,24] but not that of cells deficient for other NER components. PO and PM *K5-Terf2* keratinocytes were hypersensitive to increasing doses of MMC (**Fig. 4d**). Furthermore, MMC-treated *K5-Terf2* keratinocytes had twice as many complex chromosomal aberrations (breaks, fragments, chromatid crosslinks and tri-radials; $P \leq 0.05$ in all cases) as wild-type controls (**Supplementary Table 1** and **Supplementary Methods** online), suggesting that *K5-Terf2* cells have defective repair of DNA crosslinks, similar to that described for ERCC1-deficient cells[23]. In contrast, *K5-Terf2* keratinocytes were not more sensitive to ionizing radiation, as they showed no differences in viability or number of ionizing radiation–induced chromosomal aberrations compared with wild-type controls (**Fig. 4e** and data not shown). Taken together, these results indicate that *K5-Terf2* mice and cells are more sensitive to both UV-induced damage and DNA crosslinking agents but not to ionizing radiation.

To determine whether *K5-Terf2* mice were more susceptible to UV-induced carcinogenesis, we subjected *K5-Terf2* mice to a chronic

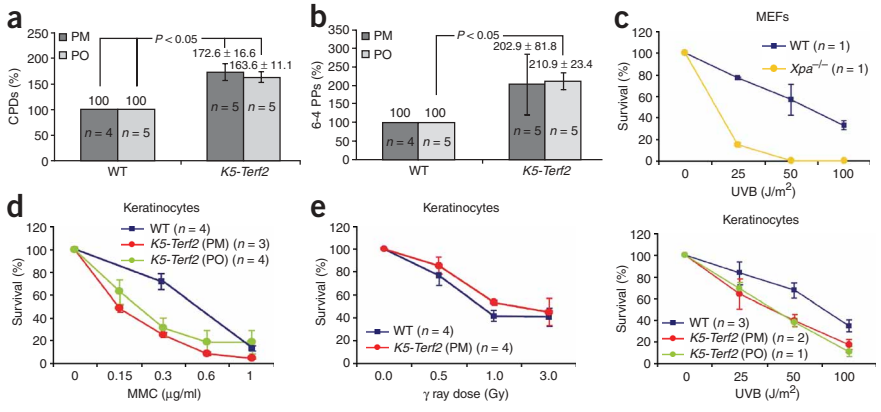

Figure 4 Hypersensitivity of *K5-Terf2* mice to UVB irradiation and MMC. (**a**,**b**) Increased CPDs (**a**) and 6-4 PPs (**b**) in genomic DNA from UVB-irradiated PM and PO *K5-Terf2* mice compared with that from wild-type littermates. Values are expressed as mean ± s.e. increase in CPDs (**a**) or 6-4 PPs (**b**) in transgenic mice relative to nontransgenic mice (n = number of mice). (**c**) Hypersensitivity of wild-type and *K5-Terf2* keratinocytes to UVB irradiation. As a control, wild-type and XPA-deficient mouse embryonic fibroblasts (MEFs) are included. Keratinocytes and mouse embryonic fibroblasts were irradiated with the indicated doses of UVB and survival was analyzed 5 d later. (**d**) Hypersensitivity of *K5-Terf2* keratinocytes to MMC treatment. Keratinocytes were treated with the indicated concentrations of MMC and survival was analyzed 5 d later. (**e**) Sensitivity of *K5-Terf2* keratinocytes to γ irradiation. Keratinocytes were irradiated with the indicated doses of γ irradiation and survival was analyzed 5 d later. (**c**–**e**) Error bars represent s.e. WT, wild-type. n = number of keratinocyte cultures.

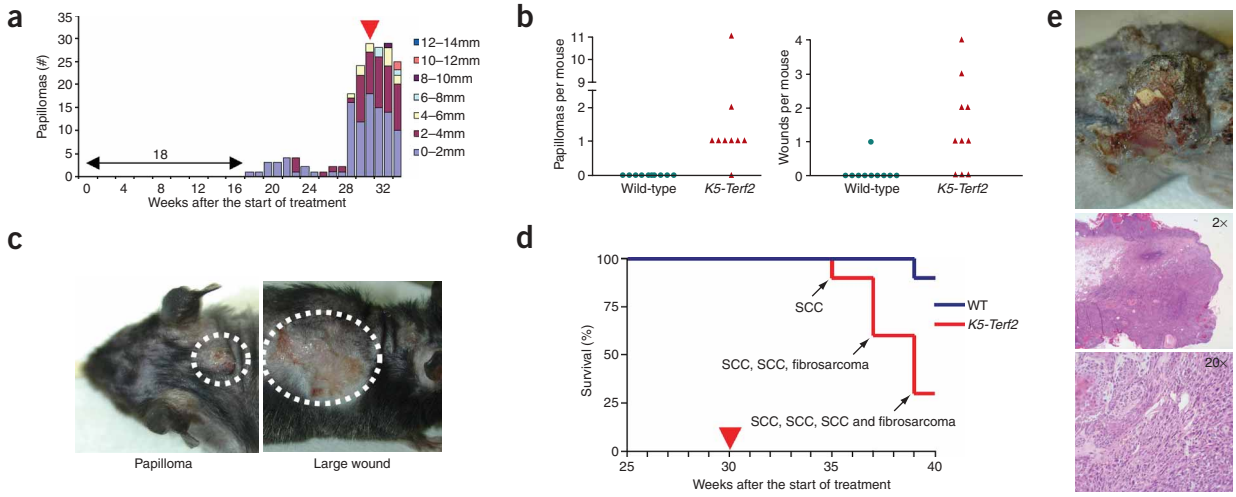

Figure 5 Increased UV-induced carcinogenesis in *K5-Terf2* mice. (**a**) Total number of papillomas in *K5-Terf2* mice ($n = 10$) after chronic UVB irradiation. Eighteen weeks after the start of the treatment, *K5-Terf2* mice developed papillomas, whereas similarly irradiated wild-type cohorts never developed papillomas (not shown). The end of treatment is indicated with an arrow. (**b**) Average number of skin papillomas and skin ulcerations per mouse 30 weeks after the start of irradiation treatment in wild-type and *K5-Terf2* cohorts ($n = 10$ each). (**c**) Representative examples of a papilloma and a large skin ulceration in a *K5-Terf2* mouse 30 weeks after the start of irradiation treatment. (**d**) Survival curve of chronically irradiated wild-type (WT; blue line) and *K5-Terf2* (red line) cohorts ($n = 10$ each). The *K5-Terf2* mice that died ($n = 7$) developed the indicated skin tumors (a full description of skin lesions is given in **Supplementary Table 2** online), whereas similarly irradiated wild-type cohorts did not develop tumors. (**e**) Different magnifications of a poorly differentiated SCC in a *K5-Terf2* mouse (PM287).

irradiation protocol, previously shown to induce tumors in mice deficient for NER components[25,26]. *K5-Terf2* mice developed papillomas and severe skin ulcerations 18 weeks after the start of the treatment, whereas similarly irradiated wild-type mice did not develop these lesions (**Fig. 5a–c**). Notably, 35 weeks after the start of the treatment, *K5-Terf2* mice developed rapidly growing skin tumors, which resulted in decreased survival of these mice compared with similarly irradiated wild-type cohorts (**Fig. 5d**). Histopathological analysis of these lesions identified different stages of skin carcinogenesis ranging from pretumoral lesions (actinic keratosis, actinic dermatitis, hyperplasia and dysplasia) to different degrees of SCCs (*in situ*, well differentiated and poorly differentiated) and fibrosarcomas (**Supplementary Table 2** online and **Fig. 5e**). These tumors were never found in similarly irradiated wild-type cohorts (data not shown). The increased UV-induced carcinogenesis in *K5-Terf2* mice, together with the occurrence of spontaneous tumors in light-exposed areas of the skin (**Fig. 2c,d**), indicate that *K5-Terf2* mice are more susceptible to UV-induced skin cancer, like individuals with xeroderma pigmentosum[17–20].

Telomere abnormalities in *K5-Terf2* mice

The premature deterioration of the skin and increased tumor incidence in light-exposed areas of the skin in *K5-Terf2* mice prompted us to study whether TRF2 expression had an effect on telomere length. We measured telomere length in *K5-Terf2* skin keratinocytes using Q-FISH on skin sections from the tail[15,16,27]. Four-month-old PM, PO and PN *K5-Terf2* mice had markedly shorter telomeres than age-matched wild-type mice (**Fig. 6a,b**), indicating that a modest increase in TRF2 levels (12 times greater in the PN line) was sufficient to provoke substantial telomere shortening *in vivo*. To address whether the telomere shortening phenotype was related to light exposure, we compared telomere length in skin from the tail (exposed to light) with that of dorsal skin (partially protected from light by hair) at different times after birth. Telomere shortening was apparent in tail skin from *K5-Terf2* mice as early as 20 days after birth, at which time the dorsal skin from these mice had normal telomeres (**Supplementary Fig. 3** online). The dorsal skin of *K5-Terf2* mice showed substantial telomere shortening only at later time points (60 days after birth; **Supplementary Fig. 3** online). These results suggest that light-exposed areas of the skin, such as the tail, have a faster rate of telomere shortening than those that are protected from light by hair, such as dorsal skin. Q-FISH analysis of metaphases from primary keratinocytes confirmed that *K5-Terf2* cells had shorter telomeres and increased frequencies of signal-free ends (telomeres without detectable TTAGGG signal) than wild-type cells (**Supplementary Fig. 4** and **Supplementary Methods** online). *K5-Terf2* cells also had significantly more end-to-end fusions lacking TTAGGG repeats at the fusion point ($P \leq 0.005$), indicating that these cells had critically short telomeres (**Supplementary Table 1** online), as well as more complex chromosomal aberrations (chromatid crosslinks, chromosomes with multiple telomeres and interstitial telomeres; $P \leq 0.005$; **Supplementary Table 1** and **Supplementary Fig. 4** online). Chromosomal instability in *K5-Terf2* keratinocytes was further aggravated with increasing culture passage compared with wild-type controls (**Supplementary Fig. 4** online). Taken together, these results indicate that increased expression of TRF2 results in telomere shortening and increased chromosomal instability.

TRF2 may have a role in protecting the G-strand overhang from degradation[6]. We determined the length of the G-strand overhang in *K5-Terf2* adult tail skin keratinocytes using native gel hybridizations (**Supplementary Methods** online). The G-strand overhang signal was markedly decreased (by >50%) in *K5-Terf2* keratinocytes compared with wild-type controls (**Fig. 6c,d** and **Supplementary Methods** online). Hybridization in denaturing conditions (**Fig. 6c**) confirmed the telomere shortening previously shown by Q-FISH (**Fig. 6a,b** and **Supplementary Fig. 4** online).

Short and dysfunctional telomeres form γH2AX DNA damage foci[28,29], a hallmark of double-strand breaks[30]. We detected a substantial increase in cells with γH2AX foci in *K5-Terf2* skin compared

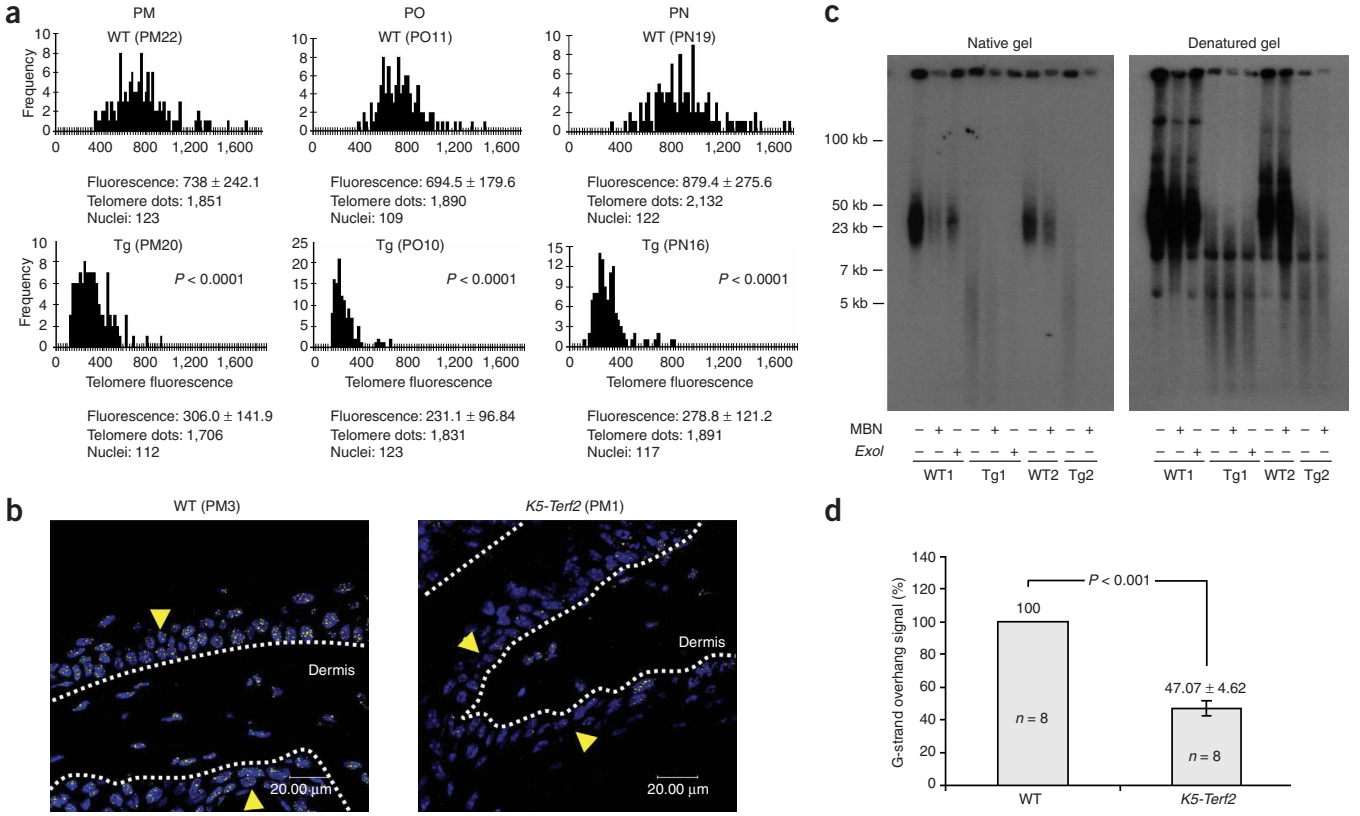

Figure 6 Telomere shortening in *K5-Terf2* mice. (**a**) Quantification of telomere fluorescence in tail skin sections from wild-type (WT) and *K5-Terf2* (Tg) mice of the indicated lines. PM20 and PM22, PO10 and PO11, and PN16 and PN19 are littermates. More than 100 keratinocyte nuclei and at least 1,700 telomere dots from each genotype were analyzed by Q-FISH. Mean ± s.d. fluorescence in arbitrary units is shown. Telomere fluorescence was significantly lower in *K5-Terf2* mice compared with the corresponding wild-type controls. (**b**) Representative images of telomere fluorescence in skin sections from wild-type (WT) and *K5-Terf2* littermates obtained using a confocal microscope. The basal layer of skin keratinocytes is indicated with yellow arrows and separated from the dermis by a white line. Telomere fluorescence was lower in basal layer skin keratinocytes from the *K5-Terf2* mouse than in those from the wild-type mouse. (**c**) Representative example of G-strand overhangs in adult skin keratinocytes from wild-type (WT) and *K5-Terf2* (Tg) mice after native gel hybridization with a $(CCCTAA)_4$ probe. After treatment with 100 units of mung bean nuclease (MBN) or 200 units of *Exo*I, the G-strand specific signal decreased by ~70%. As a control, the same gel was denatured and reprobed with the $(CCCTAA)_4$ probe to visualize telomeres. Loss of the G-strand overhang in *K5-Terf2* mice compared with wild-type littermates is indicated by the decreased signal intensity. There is marked loss of telomeric sequences in the denaturing gel. (**d**) Quantification of average G-strand overhang signals after correcting for satellite centromeric signals in *K5-Terf2* and wild-type littermate mice ($n = 8$ each). Standard error is indicated.

with wild-type skin, coincidental with a decrease in proliferating cells (Ki67-positive; **Supplementary Fig. 5** online). Furthermore, 60% of these foci colocalized with the telomeric protein TRF1, as indicated by double immunofluorescence with TRF1 and γH2AX antibodies (**Supplementary Fig. 5** and **Supplementary Methods** online), confirming that they correspond to dysfunctional telomeres.

Telomere shortening in *K5-Terf2* mice is mediated by XPF

The marked telomere shortening in *K5-Terf2* mice could result from an altered telomere structure (*i.e.*, abnormal T-loop structure), which could prevent the access of telomerase to telomeres[3,11] or result in telomere degradation. To address this question, we first generated *K5-Terf2* mice in a *K5-Tert* background with increased telomerase activity in the skin[15] (*K5-Terf2 K5-Tert* mice) and compared telomere length in the tail skin of these mice with that of *K5-Terf2* and *K5-Tert* single mutant mice. The short telomeres produced by TRF2 overexpression were not rescued in *K5-Terf2 K5-Tert* mice (**Fig. 7a**). Although these results do not rule out the possible involvement of telomerase in telomere loss in *K5-Terf2* mice, they indicate that telomerase overexpression in *K5-Tert* mice is not sufficient to prevent this phenotype. Similarly, the skin hyperpigmentation phenotype of *K5-Terf2* mice was not rescued in *K5-Terf2 K5-Tert* mice (data not shown). Next, we generated *K5-Terf2* mice in a telomerase-deficient background ($Terc^{-/-}$ mice), which have progressive telomere shortening due to lack of telomerase[31]. Tail skin of *K5-Terf2* mice and first-generation $Terc^{-/-}$ mice had shorter telomeres than that of wild-type controls (**Fig. 7b**)[27,31]. Compound mutant *K5-Terf2* $Terc^{-/-}$ mice had a further acceleration of telomere loss compared with the single mutant *K5-Terf2* and $Terc^{-/-}$ controls (**Fig. 7b**). Coincidental with shorter telomeres in *K5-Terf2* $Terc^{-/-}$ mice, the hair loss and dry skin phenotypes were exacerbated compared with age-matched *K5-Terf2* controls (data not shown), suggesting that short telomeres contribute to the development of these skin phenotypes.

Because both telomere shortening and abnormal skin phenotypes in *K5-Terf2* mice were largely dependent on exposure to light and were reminiscent of human xeroderma pigmentosum, we studied whether the XPF nuclease was responsible for telomere degradation in these mice. To this end, we generated *K5-Terf2* mice simultaneously

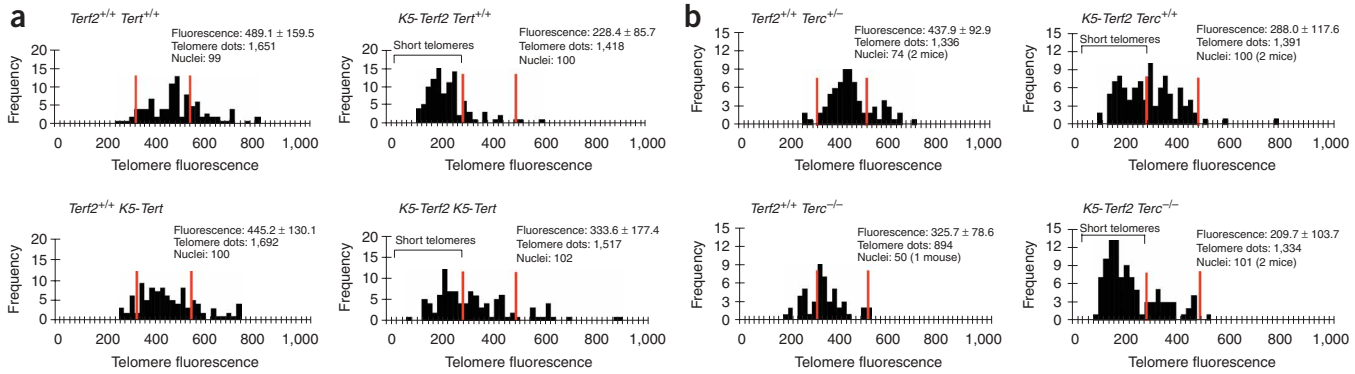

Figure 7 The short telomere phenotype of *K5-Terf2* mice is telomerase-independent. (**a**) Quantification of telomere fluorescence on tail skin sections from wild-type, *K5-Terf2 Tert*$^{+/+}$, *Terf2*$^{+/+}$ *K5-Tert* and *K5-Terf2 K5-Tert* littermate mice from the PM line. Approximately 100 keratinocyte nuclei and at least 1,400 telomere dots of each genotype were analyzed by Q-FISH. Mean ± s.d. fluorescence in arbitrary units is shown. Telomere fluorescence was significantly lower in *K5-Terf2 Tert*$^{+/+}$ and *K5-Terf2 K5-Tert* mice compared with the corresponding wild-type controls. Critically short telomeres are not rescued in the *K5-Terf2 K5-Tert* background. (**b**) Quantification of telomere fluorescence on skin sections from *Terf2*$^{+/+}$ *Terc*$^{+/-}$, *K5-Terf2 Terc*$^{+/+}$, *Terf2*$^{+/+}$ *Terc*$^{-/-}$ and *K5-Terf2 Terc*$^{-/-}$ mice. Approximately 50–100 keratinocyte nuclei and at least 800 telomere dots per genotype were analyzed by Q-FISH. $n = 1$–2 mice per genotype. Mean ± s.d. fluorescence in arbitrary units is shown. Telomere fluorescence was significantly lower in *K5-Terf2 Terc*$^{-/-}$ mice compared with *K5-Terf2 Terc*$^{+/+}$ and *Terf2*$^{+/+}$ *Terc*$^{-/-}$ controls.

deficient for XPF (encoded by *Ercc4*)[24]. *K5-Terf2 Ercc4*$^{+/+}$ mice had significantly shorter telomeres in tail skin than wild-type controls ($P < 0.0001$; **Fig. 8a**,**b**). Telomere length in *Ercc4*$^{-/-}$ single mutant mice was similar to that of wild-type controls (**Fig. 8a**,**b**), in agreement with the normal telomere length of ERCC1-deficient cells[10]. XPF deficiency largely prevented telomere shortening in compound mutant *K5-Terf2 Ercc4*$^{-/-}$ mice (**Fig. 8a**,**b**). These results indicate that telomere loss associated with TRF2 expression is dependent on the XPF nuclease, suggestive of a genetic interaction between TRF2 and XPF that is important for telomere length control. End-to-end fusions associated with critically short telomeres were also significantly prevented in *K5-Terf2 Ercc4*$^{-/-}$ cells compared with *K5-Terf2* cells ($P < 0.0001$; **Fig. 8c**), in agreement with rescue of telomere length. To assess whether XPF deficiency also rescued DNA damage associated with short telomeres in *K5-Terf2* mice, we carried out confocal immunofluorescence analysis using γH2AX antibodies directly on tail skin

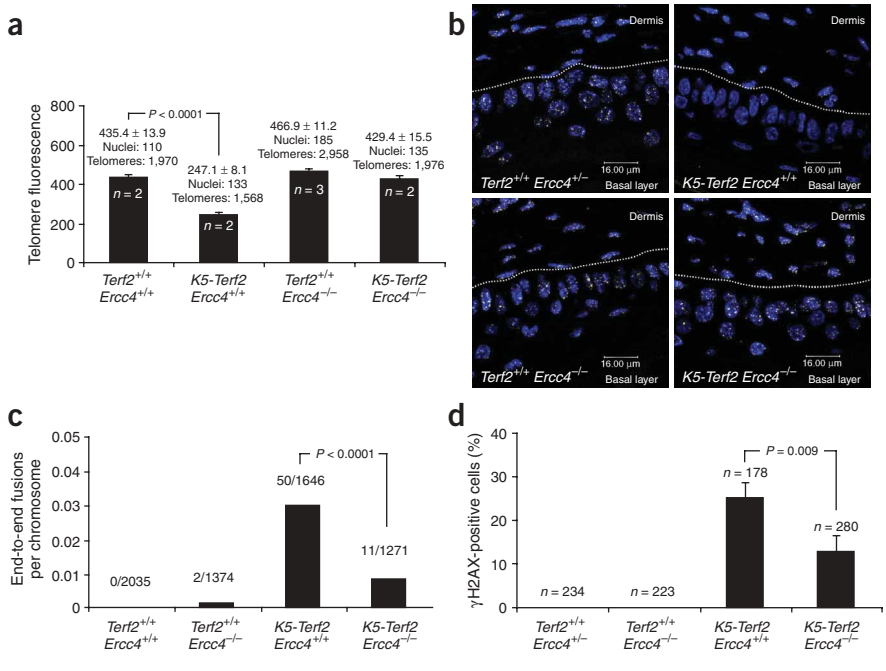

Figure 8 Telomere shortening and telomere damage in *K5-Terf2* mice is XPF-dependent. (**a**) Quantification of telomere fluorescence on tail skin sections from wild-type *Terf2*$^{+/+}$ *Ercc4*$^{+/+}$, *K5-Terf2 Ercc4*$^{+/+}$, *Terf2*$^{+/+}$ *Ercc4*$^{-/-}$ and double mutant *K5-Terf2 Ercc4*$^{-/-}$ littermate mice from the PM line. $n = 2$–3 per genotype. Approximately 100 keratinocyte nuclei and at least 1,500 telomere dots of each genotype were analyzed by Q-FISH. Mean ± s.e. fluorescence in arbitrary units is shown. *K5-Terf2 Ercc4*$^{+/+}$ mice had decreased telomere fluorescence; this telomere shortening was rescued in *K5-Terf2 Ercc4*$^{-/-}$ mice. XPF deficiency alone (in *Terf2*$^{+/+}$ *Ercc4*$^{-/-}$ mice) resulted in normal or slightly elongated telomeres relative to wild-type *Terf2*$^{+/+}$ *Ercc4*$^{+/+}$ controls. (**b**) Representative images of telomere fluorescence in tail skin sections from *Terf2*$^{+/+}$ *Ercc4*$^{+/-}$, *K5-Terf2 Ercc4*$^{+/+}$, *Terf2*$^{+/+}$ *Ercc4*$^{-/-}$ and double mutant *K5-Terf2 Ercc4*$^{-/-}$ littermate mice obtained using a confocal microscope. The dermis and basal layer are indicated and separated by a white lane. Telomere fluorescence was lower in basal layer skin keratinocytes from *K5-Terf2 Ercc4*$^{+/+}$ mice compared with *Terf2*$^{+/+}$ *Ercc4*$^{+/-}$ controls and was rescued in double mutant *K5-Terf2 Ercc4*$^{-/-}$ mice. (**c**) Frequency of end-to-end fusions per chromosome as determined by Q-FISH in mice of the indicated genotypes. A significant rescue of end-to-end fusions lacking telomeres at the fusion point was detected in *K5-Terf2 Ercc4*$^{-/-}$ mice compared with *K5-Terf2 Ercc4*$^{+/+}$ controls ($P < 0.0001$). (**d**) Quantification of total keratinocyte nuclei containing γH2AX foci in mice of the indicated genotypes. Rescue of γH2AX-positive cells was observed in *K5-Terf2 Ercc4*$^{-/-}$ mice compared with *K5-Terf2 Ercc4*$^{+/+}$ mice.

sections. XPF deficiency alone did not result in cells with increased γH2AX foci, but *K5-Terf2 Ercc4*$^{+/+}$ skin showed increased γH2AX-positive cells (**Fig. 8d**). Notably, the percentage of γH2AX-positive cells was significantly lower in *K5-Terf2 Ercc4*$^{-/-}$ skin than in *K5-Terf2 Ercc4*$^{+/+}$ skin ($P = 0.009$; **Fig. 8d**). Taken together, these results indicate that TRF2 overexpression results in rapid telomere degradation and telomere dysfunction (end-to-end fusions and γH2AX foci), both of which depend on the XPF nuclease.

DISCUSSION

K5-Terf2 mice have a severe phenotype in the skin in response to light consisting of premature skin deterioration, hyperpigmentation and increased incidence of skin tumors. These phenotypes resemble the skin pathologies of the human syndrome xeroderma pigmentosum, characterized by mutations in components of the NER pathway. *K5-Terf2* cells are hypersensitive to UV irradiation and to DNA cross-linking agents, suggesting that TRF2 has a role in the DNA damage response to these agents *in vivo*. Furthermore, *K5-Terf2* mice are more susceptible to UV-induced skin carcinogenesis, like mice deficient in components of the NER pathway[25,26]. This increased susceptibility of *K5-Terf2* mice to develop skin tumors suggests a putative role for TRF2 in skin tumorigenesis. In this regard, we show here that TRF2 is frequently altered in human skin carcinomas, highlighting the idea that TRF2 has a role in skin cancer.

In addition to an increased sensitivity to UV-induced damage, *K5-Terf2* mice have critically short telomeres and loss of the G-strand overhang preferentially in skin areas exposed to light, suggesting that there is a connection between telomere length control and UV-damage repair. We show that the XPF nuclease, involved in the NER pathway and also localized at telomeres[10], is largely responsible for the telomere degradation associated with TRF2 overexpression, genetically linking TRF2 and the NER pathway. These findings raise the possibility that the interaction between TRF2 and XPF increases XPF activity at telomeres, leading to XPF-dependent telomere loss. In turn, TRF2 may deregulate NER at nontelomeric DNA lesions resulting in increased sensitivity to UV damage.

The short telomere phenotype occurred in all the mouse lines that we tested (PN, PO and PM), whereas hyperpigmentation, skin atrophy and skin tumors were more acute in the PO and PM lines. Because these mouse lines have similarly short telomeres, we conclude that these phenotypes are not exclusively dependent on telomere length but may result from the combination of short telomeres and increased DNA damage. In support of this possibility, critically short or dysfunctional telomeres, such as in late-generation *Terc*$^{-/-}$ mice or in mice deficient for DNAPK, do not recapitulate the skin phenotypes of *K5-Terf2* mice[27,31–33]. Similarly, mice deficient in components of the NER pathway[22–26], including the XPF nuclease, with increased UV damage but normal telomere length (ref. 10 and this paper) do not reproduce the skin phenotypes of *K5-Terf2* mice. The short telomere phenotype of *K5-Terf2* mice is also characteristic of the human syndrome dyskeratosis congenita, associated with defective telomerase activity[34]. The fact that telomerase overexpression is not sufficient to rescue short telomeres in *K5-Terf2* mice suggests, however, that these mice do not have a primary defect in the telomerase pathway. TRF2 mice represent a new mouse model for evaluating the effects of telomere dysfunction in cancer and aging.

METHODS

Generation and genotyping of mice. We amplified mouse *Terf2* DNA by RT-PCR using primers 5TRF2/F and 3TRF2/R (**Supplementary Table 3** online). We sequenced an *Eco*RI-*Sal*I fragment containing the full-length mouse *Terf2* cDNA and then cloned it downstream of bovine keratin K5 regulatory sequences[14]. We purified a linear *Not*I restriction fragment containing the *K5-Terf2* transgene using QIAquick (Qiagen GmbH) and microinjected it at 2 μg μl^{-1} into the pronuclei of fertilized oocytes from C57BL/6 × CBA F_1 mice as described[15]. We identified five different founder mice by Southern-blot analysis of tail DNA, using the bovine keratin promoter as a probe. Four of the five founders (PL, PM, PN and PO) transmitted the transgene to the offspring. We backcrossed these transgenic founder mice for three to six generations onto a C57BL/6 background to obtain the different *K5-Terf2* transgenic lines studied here. We did not study the PL line because it had undetectable levels of transgene expression (data not shown). All wild-type and *K5-Terf2* mice from the different lines used here were littermates. In the PM line, only males had increased *Terf2* mRNA expression, despite the fact that both males and females carried the transgene. Crossing of PM *K5-Terf2* hemizygous transgenic males with wild-type females indicated that, in the PM line, the transgene is linked to the X chromosome and that it is selectively silenced in PM *K5-Terf2* females (data not shown).

To generate the *K5-Terf2 K5-Tert* double mutant mice, we crossed *K5-Tert* males[15] with PM *K5-Terf2* females. We genotyped the progeny by PCR using primers K5-UTR and mTRF2R1 to detect the *K5-Terf2* transgene and primers K5-UTR and Tert-TgRev to detect the *K5-Tert* transgene (**Supplementary Table 3** online). All wild-type, *K5-Terf2*, *K5-Tert* and *K5-Terf2 K5-Tert* mice used here were littermates.

To generate *K5-Terf2 Terc*$^{-/-}$ mice, we first crossed PM *K5-Terf2* males with *Terc*$^{-/-}$ females[31]. We then obtained double mutant mice by crossing *Terf2*$^{+/+}$ *Terc*$^{+/-}$ males with *K5-Terf2 Terc*$^{+/-}$ females. We detected the wild-type and mutated *Terc* alleles by Southern blotting[31].

To generate *K5-Terf2 Ercc4*$^{-/-}$ mice, we first crossed PM *K5-Terf2* males with *Ercc4*$^{+/-}$ females[24]. We then obtained double mutant mice by crossing *Terf2*$^{+/+}$ *Ercc4*$^{+/-}$ males with *K5-Terf2 Ercc4*$^{+/-}$ females. We detected the wild-type and mutated *Ercc4* alleles as described[24].

Human skin tumor samples. Human samples were provided by the Spanish National Tumour Bank Network coordinated by the Spanish National Cancer Centre, with the collaboration of Hospital "Santa María del Rosell" (Cartagena, Spain). Samples were collected in accordance with the technical and ethical procedures of the Spanish National Tumour Bank Network, including anonimization processes.

Mouse breeding and housing. Large colonies of PM, PN and PO *K5-Terf2* transgenic lines; *K5-Terf2 K5-Tert* crosses; *K5-Terf2 Terc*$^{-/-}$ crosses; and *K5-Terf2 Ercc4*$^{-/-}$ crosses were generated and maintained at the Spanish National Cancer Centre under specific pathogen-free conditions in accordance with the recommendations of the Federation of European Laboratory Animal Science Associations.

All mice described here were exposed to day-night cycles (12 h of light and 12 h of dark) at the Spanish National Cancer Centre mouse facility. The light source was white fluorescent lamps (TLD 36W/840 and TLD 58W/840, Philips), which also emit low doses of radiation between 250 nm and 400 nm, and therefore, have a component of UV light (UVA, UVB and UVC).

Western blotting. We prepared whole-cell extracts from primary keratinocytes as described[15]. We determined protein concentration using the Bio-Rad DC Protein Assay. We separated 40 μg of each extract by 8% SDS-PAGE. After transfer, we incubated the membranes with a polyclonal antibody to TRF2 (1:1,000; SF08, provided by E. Gilson, Lyon, France) and monoclonal antibody to β-actin (1:10,000; Sigma). We detected antibody binding after incubation with a secondary antibody coupled to horseradish peroxidase using enhanced chemiluminescence.

Real-time quantitative RT-PCR. We extracted total RNA using TRIzol (Invitrogen Life Technologies) from the tail and the back skin of three to five age-matched (2- to 10–month-old) wild-type and PM, PN and PO *K5-Terf2* littermates. We carried out reverse transcription with 1 μg of total RNA using random hexamers as primers and Superscript II reverse transcriptase (Invitrogen Life Technologies) in accordance with the manufacturer's instructions. We carried out real-time PCR with an ABI PRISM 7700 instrument (Applied Biosystems) using SYBR Green PCR Core Reagents (Applied Biosystems). Each

PCR reaction (15 µl) contained 1× buffer, 4 µM $MgCl_2$, 0.4 µM of each sense and antisense primer and 5 µl of the corresponding cDNA dilution. We incubated reaction mixtures for 5 min at 95 °C and then carried out 40 PCR cycles of 15 s at 95 °C, 45 s at 63 °C and 1 min and 30 s at 68 °C. Fluorescence was acquired during every 80 °C step and analyzed with the Light Cycler software. We used primers mTRF2BF and mTRF2BR, which amplified a 168-bp fragment of mouse *Terf2* cDNA (**Supplementary Table 3** online). We carried out parallel RT-PCR reactions for actin detection using primers ACTIN-F and ACTIN-R (**Supplementary Table 3** online). We determined the relative expression of TRF2 in each sample determined by calculating ΔΔCt values, which express the difference between the cycle threshold of the TRF2 primer pair and that of the β-actin primer pair. We repeated each PCR reaction two to four times to obtain the final values (**Fig. 1a**).

We carried out RT-PCR analysis of human tumors as described above using frozen tissue samples and primers hTRF2AF and hTRF2AR (**Supplementary Table 3** online), which amplified a 71-bp fragment of human *TERF2* cDNA. We determined the relative expression of TRF2 in each tumor by calculating ΔΔCt values, which express the difference between the cycle threshold of the TRF2 primer pair and that of the β-actin primer pair. We repeated each RT-PCR reaction two to three times and determined the average values (**Fig. 3a**).

Histopathology and immunohistochemistry. We fixed skin sections from 2- to 10-month-old wild-type and *K5-Terf2* mice in 10% buffered formalin, embedded them in paraffin wax, sectioned them at 4 µm and stained with hematoxylin and eosin. We captured images with a DP-10 digital camera in a Olympus Vanox microscope at the indicated magnifications.

We analyzed immunohistochemistry and immunofluorescence on skin sections after removing them from paraffin and processing them with 10 mM sodium citrate (pH 6.0) at 95 °C for 20 min. To detect Ki67, we used a streptavidin-biotin complex technique. Endogenous peroxidase activity was previously inactivated by incubation with 3% hydrogen peroxidase in methanol (15 min at room temperature), and samples were then incubated with a monoclonal antibody to Ki67 (Master Diagnostica) and with a biotinylated antibody to mouse. We obtained control slides by replacing the primary antibody with phosphate-buffered saline (PBS; data not shown). We obtained images using a Leica CTR MIC microscope.

γH2AX detection. To detect γH2AX on skin sections, we permeabilized slides in a Triton-X100 buffer at room temperature for 45 min, blocked them with 10% bovine serum albumin (Sigma) in PBS at 37 °C for 2 h and then incubated them for 2 h at room temperature with a mouse antibody to γH2AX (1:500; Upstate). After γH2AX labeling, we rinsed cells three times with PBS and 0.1% Triton-X100 and incubated them for 30 min at room temperature with goat antibody to mouse conjugated with Cy3 (1:400; Jackson Immunoresearch Laboratories, Inc.). After five rinses with PBS and 0.1% Triton-X100, we stained cells with DAPI solution. We obtained images using a confocal ultraspectral microscope (Leica TCS-SP2-A-OBS-UV).

Telomere length analyses on skin sections. For Q-FISH analysis, we removed the paraffin from paraffin-embedded skin sections from the tail or the back, hybridized them with a PNA-telomeric probe and determined telomere fluorescence as described[15,27]. We captured more than 50 keratinocyte nuclei from each mouse at 100× magnification using a Leica CTR MIC microscope and a COHU High Performance CCD camera. We integrated telomere fluorescence using spot IOD analysis in the TFL-TELO program (provided by P. Landsdorp, Vancouver, Canada). The telomere fluorescence frequencies were represented by histograms. We used confocal microscopy to visualize telomere fluorescence (**Figs. 6b** and **8b**).

UVB irradiation of mice. We shaved the backs of two to five wild-type and PM and PO *K5-Terf2* age-matched (9- to 12-weeks old) mice 24 h before exposing them to UV irradiation. We then anesthetized the mice and irradiated them with a 302-nm UVB lamp (handheld UV, UVM 57) at a fluency of 156 J m^{-2}. We killed the mice at various times after UV exposure and collected skin samples from the back (irradiated) and the abdomen (nonirradiated) of each mouse for further analyses. For analysis of CPDs and 6-4 PPs, we froze skin sections of 1 cm^2 in liquid nitrogen.

Chronic UVB carcinogenesis experiments. We shaved the back skin of 6- to 7-week-old male mice (ten wild-type and ten *K5-Terf2* mice) with electric clippers and irradiated them three times per week with UVB at a dose of 1.8 kJ m^{-2} per exposure for 30 weeks. We scored the mice for tumors once each week. We killed mice when they showed signs of poor health. We fixed skin sections in 10% buffered formalin, embedded them in paraffin and subjected them to full histopathological analysis (**Supplementary Table 2** online).

Immunodot blot analysis to quantify CPDs and 6-4 PPs. One hour after UVB irradiation, we isolated genomic DNA from skin samples from the backs and abdomens of five wild-type and five *K5-Terf2* littermate mice. We placed genomic DNA in a 1× Tris-EDTA solution, added SSPE to a final concentration of 10× and heat-denatured DNA. We then blotted DNA samples in duplicate on a positively charged nylon membrane (Hybond N+, Amersham) using a vacuum dot blot apparatus (Bio-Rad). We also blotted genomic DNA from nonirradiated skin sections (abdomen) from the same mice as a control for nonspecific DNA binding of the antibodies. We fixed DNA by baking the membrane for 15 min at 80 °C and then incubated the membrane for 1 h with a monoclonal antibody against CPDs (TDM2; 1:2,000) or with a monoclonal antibody against 6-4 PPs (64M-2; 1:100; both antibodies from T. Matsunaga, Kahazawa University, Japan). We used horseradish peroxidase–conjugated antibodies to mouse and enhanced chemiluminescence (Amersham Corp.) to detect the primary antibodies. We scanned the resulting films and quantified the signals using the NIH 1.6 software. To correct for DNA loading, we also hybridized membranes with a major satellite centromeric probe. We repeated each experiment at least three times.

MMC treatment, UV irradiation and γ irradiation of primary skin keratinocytes. We seeded 3.5 × 10^4 keratinocytes (**Supplementary Methods** online) in 12-well collagen I–precoated plates and incubated them for 24 h at 37 °C. We treated cells with different concentrations of MMC for 1 h and 30 min or irradiated them with UVB light (302 nm). For γ irradiation, we used a ^{137}Cs source (MARK 1-30 irradiator; Shepherd & Associates) at a rate of 2.11 Gy min^{-1}. After removing the medium, we washed the cells and added fresh medium. Five days after treatment, we counted viable cells using the trypan blue staining method. To analyze the effect of MMC treatment or γ irradiation on chromosomal stability, we treated cells with 0.3 µg ml^{-1} of MMC for 2 h or with different doses of γ irradiation, washed them with fresh medium and allowed them to grow for 19 h. Then we added 0.1 µg ml^{-1} of colcemide and recovered metaphases after 5 h. We prepared metaphases for Q-FISH analysis and scored chromosomal aberrations as described in **Supplementary Methods** online.

Confocal human TRF2 immunofluorescence on human skin tumor sections. We removed paraffin from human tumor sections, carried out antigen retrieval and then carried out immunofluorescence analysis of human TRF2. We permeabilized the slides in a Triton-X100 buffer at room temperature for 45 min and blocked them with 10% bovine serum albumin (Sigma) in PBS at 37 °C for 2 h. We then incubated sections for 2 h at room temperature with a mouse antibody to human TRF2 (1:200; Upstate). After human TRF2 labeling, we rinsed slides three times with PBS and 0.1% Triton-X100 and incubated them for 30 min at room temperature with goat antibody to mouse conjugated with Alexa 488 (1:200; Molecular Probes). After five rinses with PBS and 0.1% Triton-X100, we stained the slides with DAPI solution. We obtained images using a confocal ultraspectral microscope (Leica TCS-SP2-A-OBS-UV).

URLs. The technical and ethical procedures of the Spanish National Tumour Bank Network are given at http://www.cnio.es/ing/programas/progTumor01.asp.

Note: Supplementary information is available on the Nature Genetics website.

ACKNOWLEDGMENTS

We thank F.W. Alt for the XPF-deficient mice; E. Gilson for advice; M. Morente and J. García-Solano for collecting the different human tumor samples; R. Serrano for mouse work; E. Santos and J. Freire for genotyping; and M. Serrano and I. Flores for critical reading of the manuscript. P.M. is a Ramon y Cajal senior scientist. R.B. is a predoctoral fellow founded by the Spanish National Cancer Centre. The laboratory of M.A.B. is funded by

the Spanish Ministry of Education and Science, the Regional Government of Madrid, the European Union and the Josef Steiner Award 2003.

COMPETING INTERESTS STATEMENT

The authors declare that they have no competing financial interests.

Published online at http://www.nature.com/naturegenetics/
Reprints and permissions information is available online at http://npg.nature.com/reprintsandpermissions/

1. De Lange, T. Protection of mammalian telomeres. *Oncogene* **21**, 532–540 (2002).
2. Garcia-Cao, M., O'Sullivan, R., Peters, A.H., Jenuwein, T. & Blasco, M.A. Epigenetic regulation of telomere length in mammalian cells by the Suv39h1 and Suv39h2 histone methyltransferases. *Nat. Genet.* **36**, 94–99 (2004).
3. Wang, R.C., Smogorzewska, A. & de Lange, T. Homologous recombination generates T-loop-sized deletions at human telomeres. *Cell* **119**, 355–368 (2004).
4. Chan, S.W. & Blackburn, E.H. New ways not to make ends meet: telomerase, DNA damage proteins and heterochromatin. *Oncogene* **21**, 553–563 (2002).
5. Goytisolo, F.A. & Blasco, M.A. Many ways to telomere dysfunction: in vivo studies using mouse models. *Oncogene* **21**, 584–591 (2002).
6. van Steensel, B., Smogorzewska, A. & de Lange, T. TRF2 protects human telomeres from end-to-end fusions. *Cell* **92**, 401–413 (1998).
7. Bradshaw, P.S., Stavropoulos, D.J. & Meyn, M.S. Human telomeric protein TRF2 associates with genomic double-strand breaks as an early response to DNA damage. *Nat. Genet.* **37**, 193–197 (2005).
8. Zhu, X.D., Kuster, B., Mann, M., Petrini, J.H. & Lange, T. Cell-cycle-regulated association of RAD50/MRE11/NBS1 with TRF2 and human telomeres. *Nat. Genet.* **25**, 347–352 (2000).
9. Dantzer, F. *et al.* Functional interaction between Poly(ADP-Ribose) polymerase 2 (PARP-2) and TRF2: PARP activity negatively regulates TRF2. *Mol. Cell. Biol.* **24**, 1595–1607 (2004).
10. Zhu, X.D. *et al.* ERCC1/XPF removes the 3′ overhang from uncapped telomeres and represses formation of telomeric DNA-containing double minute chromosomes. *Mol. Cell* **12**, 1489–1498 (2003).
11. Smogorzewska, A. *et al.* Control of human telomere length by TRF1 and TRF2. *Mol. Cell. Biol.* **20**, 1659–1668 (2000).
12. Matsutani, N. *et al.* Expression of telomeric repeat binding factor 1 and 2 and TRF1-interacting nuclear protein 2 in human gastric carcinomas. *Int. J. Oncol.* **19**, 507–512 (2001).
13. Oh, B.-K., Kim, Y.-J., Park, C. & Park, Y.N. Up-regulation of telomere-binding proteins, TRF1, TRF2, and TIN2 is related to telomere shortening during human multistep hepatocarcinogenesis. *Am. J. Pathol.* **166**, 73–80 (2005).
14. Murillas, R. *et al.* Expression of a dominant negative mutant of epidermal growth factor receptor in the epidermis of transgenic mice elicits striking alterations on hair follicle development and skin structure. *EMBO J.* **14**, 5216–5223 (1995).
15. González-Suarez, E. *et al.* Increased epidermal tumors and increased skin, wound healing in transgenic mice overexpressing the catalytic subunit of telomerase, mTERT, in basal keratinocytes. *EMBO J.* **20**, 2619–2630 (2001).
16. González-Suárez, E., Flores, J.M. & Blasco, M.A. Cooperation between p53 mutation and high telomerase transgenic expression in spontaneous cancer development. *Mol. Cell. Biol.* **22**, 7291–7301 (2002).
17. de Boer, J. & Hoeijmakers, J.H. Nucleotide excision repair and human syndromes. *Carcinogenesis* **21**, 453–460 (2000).
18. Berneburg, M. & Lehmann, A.R. Xeroderma pigmentosum and related disorders: defects in DNA repair and transcription. *Adv. Genet.* **43**, 71–102 (2001).
19. de Laat, W.L., Jaspers, N.G. & Hoeijmakers, J.H. Molecular mechanism of nucleotide excision repair. *Genes Dev.* **13**, 768–785 (1999).
20. Petit, C. & Sancar, A. Nucleotide excision repair: from *E. coli* to man. *Biochimie* **81**, 15–25 (1999).
21. Mu, D. *et al.* DNA interstrand cross-links induce futile repair synthesis in mammalian cell extracts. *Mol. Cell. Biol.* **20**, 2446–2454 (2000).
22. McWhir, J., Selfridge, J., Harrison, D.J., Squires, S. & Melton, D.W. Mice with DNA repair gene (ERCC-1) deficiency have elevated levels of p53, liver nuclear abnormalities and die before weaning. *Nat. Genet.* **5**, 217–224 (1993).
23. Weeda, G. *et al.* Disruption of mouse ERCC1 results in a novel repair syndrome with growth failure, nuclear abnormalities and senescence. *Curr. Biol.* **7**, 427–439 (1997).
24. Tian, M., Shinkura, R., Shinkura, N. & Alt, F.W. Growth retardation, early death, and DNA repair defects in mice deficient for the nucleotide excision repair enzyme XPF. *Mol. Cell. Biol.* **24**, 1200–1205 (2004).
25. Nakane, H. *et al.* High incidence of ultraviolet-B or chemical-carcinogen-induced skin tumors in mice lacking the xeroderma pigmentosum group A gene. *Nature* **377**, 165–168 (1995).
26. Sands, A.T., Abuin, A., Sánchez, A., Conti, C.J. & Bradley, A. susceptibility to ultraviolet-induced carcinogenesis in mice lacking XPC. *Nature* **377**, 162–165 (1995).
27. González-Suárez, E., Samper, E., Flores, J.M. & Blasco, M.A. Telomerase-deficient mice with short telomeres are resistant to skin tumorigenesis. *Nat. Genet.* **26**, 114–117 (2000).
28. d'Adda di Fagagna, F. *et al.* A DNA damage checkpoint response in telomere-initiated senescence. *Nature* **426**, 194–198 (2003).
29. Takai, H., Smogorzewska, A. & de Lange, T. DNA damage foci at dysfunctional telomeres. *Curr. Biol.* **13**, 1549–1556 (2003).
30. Modesti, M. & Kanaar, R. DNA repair: spot(light)s on chromatin. *Curr. Biol.* **11**, R229–R232 (2001).
31. Herrera, E. *et al.* Disease states associated to telomerase deficiency appear earlier in mice with short telomeres. *EMBO J.* **18**, 2950–2960 (1999).
32. Vogel, H., Lim, D.S., Karsenty, G., Finegold, M. & Hasty, P. Deletion of Ku86 causes early onset of senescence in mice. *Proc. Natl. Acad. Sci. USA* **96**, 10770–10775 (1999).
33. Espejel, S. *et al.* Shorter telomeres, accelerated ageing and increased lymphoma in DNA-PKcs-deficient mice. *EMBO Rep.* **5**, 503–509 (2004).
34. Bessler, M., Wilson, D.B. & Mason, P.J. Dyskeratosis congenita and telomerase. *Curr. Opin. Pediatr.* **16**, 23–28 (2004).